Laser-Assisted Design of MOF-Derivative Platforms from Nano- to Centimeter Scales for Photonic and Catalytic Applications

Ekaterina V Gunina, Nikolaj A Zhestkij, Maksim Sergeev, Semyon V Bachinin, Yuri A Mezenov, Nikita K Kulachenkov, Maria Timofeeva, Valentina Ivashchenko, Alexander S Timin, Sergei A Shipilovskikh, et al.

Laser-Assisted Design of MOF-Derivative Platforms from Nano to Centimeter Scales for Photonic and Catalytic Applications

Ekaterina V. Gunina,[1†] Nikolaj A. Zhestkij,[1†] Maksim Sergeev,[1] Semyon V. Bachinin,[1] Yuri A. Mezenov,[1] Nikita K. Kulachenkov,[1‖] Maria Timofeeva,[1] Valentina Ivashchenko,[1] Alexander S. Timin,[1] Sergei A. Shipilovskikh,[1] Anastasia A. Yakubova,[2] Dmitry I. Pavlov,[3] Andrei S. Potapov,[3] Jiang Gong,[4] Laura Khamkhash,[5] Timur Sh. Atabaev,[5] Stéphanie Bruyere,[6] Valentin A. Milichko[1,6]*

[1] School of Physics and Engineering, ITMO University, St. Petersburg, 197101, Russia

[2] Peter the Great St. Petersburg Polytechnic University, St. Petersburg 195251, Russia

[3] Nikolaev Institute of Inorganic Chemistry SB RAS, Novosibirsk 630090, Russia

[4] Key Laboratory of Material Chemistry for Energy Conversion and Storage, School of Chemistry and Chemical Engineering, Huazhong University of Science and Technology, Wuhan 430074, China

[5] Department of Chemistry, Nazarbayev University, Astana 010000, Kazakhstan

[6] Université de Lorraine, CNRS, IJL, F-54011 Nancy, France

* E-mail: valentin.milichko@univ-lorraine.fr

† Equal contribution

‖ Present address: Department of Mechanical Engineering, Tufts University, Medford, USA

KEYWORDS. Metal-organic framework, laser ablation, MOF derivatives, nanoparticles, surface, nonlinear optics, catalysis.

ABSTRACT. Laser conversion of metal-organic frameworks (MOFs) has been recently emerged as fast and low-energy consumptive approach to create scalable MOF derivatives for catalysis, energy, and optics. However, due to the virtually unlimited MOF structures and tunable laser parameters, the results of their interaction are unpredictable and poorly controlled. Here we experimentally base a general approach to create nano to centimeter scale MOF derivatives with the desired nonlinear optical and catalytic properties. Five three- and two-dimensional MOFs, differing in chemical composition, topology and thermal resistance, have been selected as precursors. Tuning the laser parameters (i.e., pulse duration from fs to ns and repetition rate from kHz to MHz), we switch between ultrafast non-thermal destruction and thermal decomposition of MOFs. We have established that, regardless of the chemical composition and MOF topology, the tuning of the laser parameters allows obtaining a series of structurally different derivatives, as well the transition from fs to ns laser regimes ensures the scaling of the derivatives from nano to centimeter scales. Herein, the thermal resistance of MOFs effects on the structure and chemical composition of the resulting derivatives. Finally, we outline the "laser parameters vs. MOF structure" space, in which one can create the desired and scalable platforms with nonlinear optical properties from photoluminescence to light control and enhanced catalytic activity.

1. INTRODUCTION

Metal-organic frameworks (MOFs) have been recently emerged as a new paradigm in crystal engineering.[1-3] Combining organic and inorganic building blocks, packed into well-defined structures supported by strong and weak bonds, MOFs exhibit unprecedented porosity[4] along with a structural order and chemical diversity.[5] On the one hand, metal-organic nature and complex hierarchy provide MOF with gas storage and separation properties, energy storage, catalysis, drug delivery, sensing, and even photonic applications.[6-11] On the other hand, these specific properties allow MOF utilization as precursors for obtaining new forms of artificial nanostructures and derivatives,[12-16] which are inaccessible to be obtained by classical bottom-top fabrication techniques.[17-19] In turn, the resulting derivatives exhibit exceptional catalytic, capacitive, and optical properties, being nonspecific for their precursor analogs.

From a manufacturing point of view, the most common approach to fabricate MOF derivatives is thermal decomposition through holding the MOF powders at an elevated temperature (up to 1000 °C) for several hours in an oven.[20-23] However, recent studies have shown an alternative, fast and low-energy consumptive approach. Since MOFs are able to absorb laser energy efficiently and then transfer it into the heat, an intense laser irradiation stimulates fast decomposition of MOFs and their building blocks rearrangement at ambient conditions. Such laser-assisted conversion[24] (referring in the literature also as the laser metallurgy,[25] manufacturing,[26] annealing,[27] scribing, or even ablation[28]) makes it possible to fabricate scalably the MOF derivatives in real time for optical, electronic and catalytic applications.[25-32] However, due to a huge variety of MOF structures (more than 1.000.000 registered compounds in CCDC) and tunability of the laser parameters (wavelength, pulse fluence and duration), the result of the interaction of intense laser light and MOF is yet unpredictable and poorly controllable.

Here we report on the laser-assisted rational design of MOF derivatives with the desired structure, composition, scale, and corresponding nonlinear optical and catalytic properties. The concept is based on the precise control of thermal effect of the laser radiation on MOF structure allowing one to operate in either ultrafast non-thermal destruction or the thermal decomposition regimes (i.e., conversion of initial MOFs into derivatives of varied structure and functionality). Using four commercially available 3D MOFs (HKUST-1, ZIF-8, ZIF-67, and UiO-66) and 2D MOF ($\{[Zn(tr_2btd)(bpdc)]\cdot DMF\}_n$, where tr_2btd = 4,7-di(1H-1,2,4-triazol-1-yl)-2,1,3-benzothiadiazole and bpdc = 4,4′-biphenyldicarboxylate)[33] with different structures, chemical compositions and thermal resistance (Table S1), we have discovered the general rules for the laser conversion of MOFs into the desired nano and centimeter scale derivatives via tuning the laser parameters (pulse duration from fs to ns and repetition rate from kHz to MHz) and the MOF structures (**Figure 1**). We reveal that the tuning of the laser parameters (from ns to fs) allows extending a series of MOF derivatives from carbon aggregates, carbon aggregates with metal and/or metal oxide nanocrystals, to MOF nanocrystals, amorphous metal-organic nanoparticles with intact ligands, and metal-organic nanoparticles containing metal and/or metal-oxide nanocrystals. Finally, the resulting MOF derivatives exhibit distinctive optical properties for targeted applications from photoluminescence of nanometer scale derivatives to modulated photoluminescence from adsorbed dyes and the catalytic activity of the 4 cm^2 surface of MOF derivatives.

2. MATERIALS and METHODS

2.1 Laser Conversion. In general, laser conversion (including ablation) is a well-known process for transforming different materials into a variety of structures for applications ranging from catalysis to photonics. Herein, the time of laser exposure to the material is one of the key criteria

affecting the yield. Depending on this time, it is customary to divide the laser conversion (also ablation) into two opposite processes, which differ fundamentally in the mechanisms of material modification. The first, so-called "cold" laser ablation, is typical for the action of ultrashort laser pulses with a photon energy exceeding the chemical binding energy of the material. In this case, the ablation of the material causes its ionization, followed by the breaking of the chemical bonds in a time shorter than the electron-phonon relaxation. However, when the energy of such ultrashort laser pulses is insufficient for ionization, an increase in the laser intensity can lead to a multiphoton absorption process. When the intensity exceeds app. TW/cm^2, the ablation process causes a huge amount of valence electrons to be detached via Zener tunneling.[34] Then, due to the relative inert reaction of the material, the ionization occurs, followed by hydrodynamic expansion. Here, some authors advocate for the phenomenon of the Coulomb explosion.[35] In contrast, when the duration of the laser pulse, interacting with the material, is comparable to the electron-phonon relaxation time (ps to ns),[36] an opposite ablation process is observed. In this case, electrons and phonons are out of thermodynamic equilibrium. Thermalization of electrons due to electron-electron interaction in fractions of picoseconds leads to a new Fermi distribution; while electron-phonon interaction in picoseconds leads to an increase in the temperature of the material. The latter leads to material modification caused by so-called "hot" laser ablation.

Apart from the laser conversion (ablation) of inorganic materials,[37,38] the use of organics for producing different photonic and medical structures is also widespread.[39] However, the laser conversion,[24] metallurgy,[25] manufacturing,[26] annealing,[27] scribing, or even ablation[28] of hierarchical metal-organic materials like MOFs have been started less than 4 years ago.[25,32] Nevertheless, these results are highly promising for both photonics, electronics, and catalysis. Indeed, the laser conversion of MOFs makes it possible to obtain complex and even unique

forms of nanomaterials such as metal oxides,[24,26] carbides[40] and sulfides,[41] multicomponent alloys,[28,31,42-44] carbon,[29] metal-carbon and organometallic nanostructures,[30,32,45] as well as to initiate the structural defects[46] and laser writing.[25,27,47] Most of these works have been carried out in the nanosecond laser regime, paying special attention to the effect of the initial structure and composition of the MOF precursors[24-32,40-45,48] and the laser power[24,25,27,30,40,43] on the decomposition yield.

2.2 MOF Selection. In our work, we have considered the "cold", "hot", and intermediate laser conversion regimes for four representative 3D MOFs based on Cu, Zn, Co, and Zr and organic ligands like benzene-1,3,5-tricarboxylic acid, 2-methylimidazole, and 1,4-benzodicarboxylic acid (i.e., HKUST-1, ZIF-8, ZIF-67, and UiO-66), as well as for 2D MOF based on Zn, tr_2btd and bpdc ligands.[33] The selected MOFs differ in their structure and thermal resistance (Table S1 and SI, Part VI). Since the thermal decomposition of MOFs is generally the result of the breaking of bonds between metal ions and organic ligands, their thermal resistance is related to the strength and the number of these bonds. Moreover, the decomposition can also take the form of MOF amorphization and/or melting.[49] For the selected MOF like HKUST-1, the average thermal decomposition temperature is quite low and usually ranges from 250 to 300 °C.[50] Regarding ZIFs, due to their similarity to the crystalline zeolites, a good thermal resistance up to 300 - 400 °C can be observed.[51] In contrast, UiO-66 demonstrates excellent thermal resistance: the decomposition temperature ranges from 425 to 600 °C depending on the environmental conditions (see details in SI, Part VI).[52] The selected 2D MOF shows an average value of the thermal resistance (320 °C)[33] close to ZIF series.

Then, the selected MOFs have been subjected to the laser conversion (see Methods in SI). For this, the single MOF crystals with an average thickness of 100 μm (for HKUST-1), 40 μm (for

ZIF-67 and UiO-66), and 5 μm (for ZIF-8) have been placed on glass or indium tin oxide (ITO) substrate. The laser radiation (100 ns laser pulses with a center wavelength of 1070 nm, and 200 fs laser pulses with a center wavelength of 1030 nm) has been focused on the single MOF crystal using an objective (Mitutoyo 50x or 10x). The repetition rate of the laser pulses for fs radiation was set at 1 kHz and 1 MHz; while for ns radiation, a 10 kHz repetition rate has been chosen. The laser fluence has been varied from several μJ cm^{-2} to J cm^{-2} regardless the laser pulse duration (see SI, Part I). During the laser conversion of MOFs, the products (i.e., MOF derivatives: HKUST-1 DER, ZIF-8 DER, ZIF-67 DER, UiO-66 DER, and 2D MOF DER) have been deposited on the same glass or ITO substrate (or carbon grid). Then, the resulting MOF derivatives have been subjected to morphological, structural, elemental, and optical analysis using scanning and transmission electron microscopy (SEM, TEM), fast-Fourier-transformation (FFT) in high-resolution TEM (HRTEM) mode, energy-dispersive X-ray spectroscopy (EDX), powder X-Ray diffraction (PXRD) analysis, atomic force microscopy (AFM), as well as Raman, optical, photoluminescence (PL) confocal microspectroscopy, and catalytic analysis.

3. RESULTS and DISCUSSION

3.1 HKUST-1. The results of the laser conversion of HKUST-1 single crystals have been summarized in **Figure 2A1-E1** (and Figures S1, S4). As one can see, fs laser light (fs, 1 kHz) allows conversion the MOF into the melted particles (HKUST-1 DER (fs, 1 kHz)), consisting mainly of metal oxide with the presence of a sufficient amount of carbon, as confirmed by TEM, FFT (Figure S8, Table S3), EDX (Figure S4) and Raman analysis in **Figure 3A-C**. An increase in the repetition rate of fs laser pulses (fs, 1 MHz) did not significantly change the results of the conversion: the amorphous particles of metal oxide with the presence of carbon are usually detected (Figure S9, Table S4). However, ns laser regime (ns, 10 kHz) made it possible to obtain

a larger amount of pure metal (metal-oxide, to less extent) particles coated with a thick carbon shell, as seen from the Raman analysis in Figure 3C:[53] intense peaks in the region of 100 - 250 cm^{-1}, corresponding to the Cu-O bond, and pronounced D, G carbon peaks centered at 1320 and 1600 cm^{-1}.[54] Statistical analysis of the obtained MOF derivatives also showed that increasing the pulse duration from 200 fs to 100 ns does not affect their size distribution (Figure S1): 50 ± 10 nm size of the particles is observed for the (fs, 1 kHz) and (fs, 1 MHz) regimes (with the maximum size of 600 nm); and for the (ns, 10 kHz) regime, 40 ± 20 nm particles are detected (with the maximum size of 300 nm).

3.2 ZIFs. Conversion of ZIF series, an intermediate between the MOFs with high and low thermal resistance, showed the following. For ZIF-67 (Figure 2A2-E2, S2), fs laser regime (fs, 1 kHz) makes it possible to obtain the fragments of the crystal itself with the presence of metal oxide and some amorphization (Raman results on Figure 3D, EDX in Figure S5, and FFT in Figure S10). Increasing the repetition rate of the fs laser pulses (fs, 1 MHz) led to the appearance of completely amorphous particles (Figure S11 and 3D). The ns laser conversion (ns, 10 kHz), as in the case of HKUST-1, leads to the formation of metal/metal-oxide particles (as confirmed by Raman, Figure 3D), covered with a carbon shell. For ZIF-8 (Figure 2A3-E3, S2), fs laser regime (fs, 1 kHz) with an increased laser fluence (Table S2)[55] results in the creation of the crystal fragments and some amorphous particles. Increasing the repetition rate of the fs laser pulses (fs, 1 MHz) leads to sufficient particle amorphization (**Figure 4A-C** and FFT in Figure S12). Again, the ns laser conversion (ns, 10 kHz), as in the case of HKUST-1 and ZIF-67, leads to the formation of metal/metal-oxide particles covered with a thick carbon shell (as confirmed by Raman, Figure 4C, and EDX, Figure S5). In contrast to HKUST-1 (Figure S1), the statistical analysis of the obtained ZIF-67 and ZIF-8 derivatives showed that increasing the pulse duration

from 200 fs to 100 ns affects their size distribution (Figure S2): 50 ± 20 nm size of the particles is detected for both MOFs at the (fs, 1 kHz) regime (with the maximum size of 1200 nm); (fs, 1 MHz) regime provides 50 ± 10 nm and 25 ± 20 nm (and also 120 ± 10 nm) size of the particles for ZIF-67 and ZIF-8, respectively (with the maximum size of 400 nm); and for the (ns, 10 kHz) laser regime, 100 ± 50 nm and 50 ± 30 nm size of the particles is detected for ZIF-67 and ZIF-8, respectively (with the maximum size of 1000 nm).

3.3 UiO-66. In contrast, UiO-66 demonstrates a high resistivity of the organic part to fs and ns laser conversion, producing UiO-66 DER with more complex structure and morphology (Figure 2A4-E4, S3). Indeed, fs laser conversion (fs, 1 kHz) produces the crystal fragments with insufficient amorphization (as confirmed by Raman in Figure 4D, and powder X-Ray diffraction in Figure S16); while an increasing the repetition rate of the fs laser pulses (fs, 1 MHz) stimulates the amorphization and forms inclusions of metal-oxide particles (EDX in Figure S6, FFT results in Figures S13-S15, and Table S5). The ns laser regime (ns, 10 kHz) still preserves the integrity of the ligand and MOF structure (see Raman spectrum in Figure 4D for UiO-66 DER (ns, 10 kHz), and powder X-Ray diffraction in Figure S16), allowing observation mostly the amorphous organic particles containing metal-oxide (Figure S6) with some carbon contamination. Here, as in the case of HKUST-1, the statistical analysis of the obtained MOF derivatives also showed that increasing the pulse duration from 200 fs to 100 ns does not affect their size distribution (Figure S3): 50 ± 40 nm, 50 ± 20 nm, and 50 ± 20 nm size of the particles is observed for the (fs, 1 kHz), (fs, 1 MHz), and (ns, 10 kHz) laser regimes, respectively (with the maximum size of 1200 nm).

3.4 2D MOF. We also confirmed a similar dependence of morphology, size, and composition of the MOF derivatives for the selected 2D MOF. The (fs, 1 kHz) laser regime provides the

shapeless and dendrite-like[32] amorphous particles of 40 ± 20 nm size (Figure S1), consisting mainly of metal-oxide with the presence of organic ligand, as confirmed by TEM (Figure S7), EDX (Figure S4) and Raman analysis (Figure S18). An increase in the repetition rate of fs laser pulses (fs, 1 MHz) led to obtain also the shapeless amorphous particles of 60 ± 40 nm size (Figure S1), consisting mainly of metal-oxide (Figure S4, S18). Finally, ns laser regime (ns, 10 kHz) made it possible to obtain smaller particles (15 ± 10 nm) of the metal oxide and the presence of carbon (Figure S1, S4, and S18).

3.5 Photoluminescence. The results of the structural analysis are in good agreement with ones of the PL for the MOF derivatives. **Figure 5** shows that the fs laser conversion of the MOFs with the high thermal resistance slightly changes the spectrum of PL (i.e., for UiO-66 DER in comparison with the initial MOF crystal). For less thermally stable frameworks, ZIF-8 DER demonstrates the blue shifted PL spectrum; 2D MOF DER shows the red shifted PL (Figure S17); while ZIF-67 DER and HKUST-1 DER did not show any PL emission. However, the ns laser regime, regardless of the MOF structure and chemical composition, makes it possible to obtain the derivatives with the same PL spectra (pumped with 400 nm), similar to that of carbon and its allotropic forms.[56]

3.6 Laser Parameters vs MOF Structure. Taking into account the thermal resistance of the MOFs and the laser conversion parameters, the results of electronic and optical spectroscopy (Figures 2-5) for the derivatives can be represented as follows (**Figure 6D**). An increase in the thermal resistance of the MOFs subjected to (fs, 1 kHz) laser regime makes it possible to obtain structures from amorphous carbon particles with a metal or metal-oxide impurity to crystal fragments with a low degree of amorphization. On the contrary, (ns, 10 kHz) laser conversion regime of the MOFs with an increased thermal resistance makes it possible to obtain the

structures from pure carbon and metal or metal-oxide particles to amorphous organometallic particles with metal-oxide inclusions. With such a harsh laser conversion regime, the integrity of the ligand is almost never observed (a rare exception for UiO66, Figure 4D). At the same time, the intermediate laser conversion regime (i.e., fs, 1 MHz) gives the results balancing between the "hot" and "cold" laser ablation, making it possible to obtain both metal and metal oxide particles with a carbon shell and metal oxide particles with an organic shell, and even crystal fragments with significant amorphization. This analysis made it possible to outline the "laser parameters vs. MOF structure" space for predicting the results of laser-assisted design of MOF derivatives.

In addition, we have found that the laser conversion of HKUST-1 above the threshold fluence of 10 μJ cm^{-2} (for ns, 10 kHz) and 0.1 mJ cm^{-2} (for fs, 1 MHz) was accompanied by the emission of white light (Figure 6D). We speculate here about the emission of a black body heated to several thousand K.[25] Nevertheless, the laser conversion products have also been formed, corresponding to the MOF derivatives from Figure 2E.

3.7 Application, Part I. Using the "laser parameters vs. MOF structure" space, we have selectively chosen an opposite MOFs (in terms of the thermal resistance, Table S1) and applied separately two opposite laser conversion regimes (fs, 1 kHz; and ns, 10 kHz) to obtain scalable derivatives. As one can see in Figure 6A, the laser conversion (fs, 1 kHz) of UiO-66 makes it possible to obtain nanometer scale particles (up to 100 nm in diameter for UiO-66 DER), demonstrating the PL signal, partly inherent in their bulk counterparts. The size of UiO-66 DER obtained contributes to the PL enhancement for potential light control at the nanoscale.[32] On the other hand, the (ns, 10 kHz) laser conversion regime of such MOFs will make it possible to obtain scalable surfaces consisting of amorphous organics with metal-oxide inclusions, which are potentially useful for data storage application.[57]

At the same time, the scalable laser conversion of HKUST-1 (regardless of the regime) has been performed in reflection geometry for 0.5 mm thin film consisting of pressed HKUST-1 microcrystals on a fused silica substrate. This allows obtaining 4 cm^2 surface (Figure 6C) of different ratio of carbon and pure metal (Cu) inclusions, which demonstrates a similar optical reflection behavior as bulk infrared Cu mirror (Figure 6B).[58] It should be noted that the optical properties of the derivatives from such optically active and structurally adaptive MOFs, such as UiO-66 and HKUST-1, both fundamentally and technologically differ from the precursor analogs used for nonlinear optics. [59-61]

3.8 Application, Part II. The surfaces obtained from the laser conversion of HKUST-1 in Figure 6C turned out to be promising also for detection and control the fluorescently labeled biomolecules. To demonstrate this, on the one hand, we used their metallic nature and created a series of 4 cm^2 surfaces by fs laser conversion of HKUST-1 with 100 kHz, 500 kHz and 1 MHz repetition rates (the resulting roughness of which is approximately the same, Figure S20). The SEM micrographs of the developed surfaces are presented in **Figure 7A,B**. We assumed that the copper nature of such centimeter scale derivatives will be able to modulate the intensity of the PL signal from adsorbed fluorescent biomolecules in the region of 580 nm.[62] For this, we have covered the surfaces by bovine serum albumin (BSA) conjugated with cyanine 5 (Cy5) and fluorescein isothiocyanate (FITC) dyes for bright fluorescence centered at 675 nm (BSA-Cy5) and 530 nm (BSA-FITC). In details, 10 μl of BSA-Cy5 or BSA-FITC was added to the surface, followed by drying at 40 °C for 20 min. Then the resulting surfaces have been analyzed by confocal laser scanning microscopy (CLSM) with 633 nm (for BSA-Cy5) and 488 (for BSA-FITC) nm laser pump (Figure 7C,D). As a reference, we have also used gold film covered by BSA-Cy5 and BSA-FITC conjugates, prepared and analyzed under the same conditions. As one

can see on Figure 7F, a detailed analysis of the Cy5 system showed PL emission in the region of 675 nm for the gold film and the surfaces; while statistically we have found that the intensity of PL from HKUST-1 DER (fs, 1 MHz) surface is 2 times higher compared with gold and HKUST-1 DER (fs, 100 kHz) surfaces. This can be explained by the formation of a larger number of metallic elements during the fs laser conversion at an enhanced repetition rate. In this case, we have also observed an increase in PL intensity in the region of Cu plasmon resonance for the surfaces. Regarding the FITC system (Figure 7E), we have observed similar shape of the PL spectra on different surfaces; however, HKUST-1 DER (fs, 100 kHz) surface provided PL signal on average 5 times greater than gold and HKUST-1 DER (fs, 1 MHz) surfaces.

Continuing the story of the metallic-carbon nature of the surfaces based on HKUST-1, we have also tested their catalytic activity[63] using the decomposition of dyes (Figure 7G,H). For this, 2 mL of Rhodamine 800 (Rh800) aqueous solution (62.5 mg L^{-1}, 0.126 mmol) and the surfaces (100 kHz, 500 kHz, and 1 MHz) were charged in a beaker. Then 0.1 mL H_2O_2 (30 % wt) aqueous solution was added and kept at room temperature for 24 hours. The content of Rh800 in the solution was determined by Shimadzu UV-3600 ultraviolet spectrometer in 0, 1, 2, 4, 8 and 24 hours. An aqueous solution of Rh800 (62.5 mg L^{-1}) with 0.1 ml of H_2O_2 (30% wt) served as a reaction control. As one can see (Figure 7G,H), a twofold increase in the reaction rate is observed for the surface HKUST-1 DER (fs, 100 kHz), while a more metallized (via fs, 1 MHz) surface and the control show similar results. Thus, photocatalitic degradation of Rh800 showed that HKUST-1 DER (fs, 100 kHz) surface provided the most significant photocatalityc activity compared to HKUST-1 (fs, 500 kHz, 1 MHz) with the same surface roughness (Figure S20) and the control experiments.

4. CONCLUSION

We report on statistical analysis of different processes of interaction of laser light with metal-organic frameworks and establish the general concept for the controlled laser-assisted design of nano to centimeter scale MOF derivatives with the desired nonlinear optical and catalytic properties. Five representative 3D and 2D MOFs, differing in chemical composition, topology and thermal resistance, have been selected as precursors. Tuning the laser parameters (duration of the laser pulses from fs to ns and their repetition rate from 1 kHz to 1 MHz), we discovered two distinct regimes of light-matter interaction: ultrafast non-thermal destruction and thermal decomposition through the laser metallurgy. We have discovered that, regardless of the chemical composition and MOF topology, the tuning of the laser parameters (from ns to fs) allows extending a series of MOF derivatives from carbon aggregates, carbon aggregates with metal and/or metal oxide nanocrystals, to MOF nanocrystals, amorphous metal-organic nanoparticles with intact ligands, and metal-organic nanoparticles containing metal and/or metal-oxide nanocrystals (Figure 1). In addition, regardless of the composition and MOF topology, the transition from fs to ns laser pulses ensures the scaling of specific MOF derivatives from nano to centimeter scales. Herein, the thermal resistance of MOF precursors directly effects on the structure and chemical composition of the resulting derivatives. The statistical analysis of the MOF derivatives by electronic and optical spectroscopy made it possible to outline the "laser parameters vs. MOF structure" space (Figure 6D), in which one can create the materials with the desired structure and functionality. The resulting scalable MOF derivatives with the controlled structure have shown exceptional optical properties from photoluminescence of single nanometer scale MOF derivatives to modulated photoluminescence from adsorbed dyes and enhanced catalytic activity of the 4 cm^2 surface of MOF derivatives.

ASSOCIATED CONTENT

Supporting Information. The following files are available free of charge: Methods description, SEM, EDX, statistical analysis of size distribution, TEM, FFT, PXRD, AFM, and optical spectra (PDF).

AUTHOR INFORMATION

Corresponding Author

Valentin A. Milichko – School of Physics and Engineering, ITMO University, St. Petersburg, 197101, Russia; Université de Lorraine, CNRS, IJL, F-54011 Nancy, France; ORCID: 0000-0002-8461-0804; E-mail: valentin.milichko@univ-lorraine.fr.

Authors

Ekaterina V. Gunina – School of Physics and Engineering, ITMO University, St. Petersburg, 197101, Russia

Nikolaj A. Zhestkij – School of Physics and Engineering, ITMO University, St. Petersburg, 197101, Russia

Maksim Sergeev – School of Physics and Engineering, ITMO University, St. Petersburg, 197101, Russia

Semyon V. Bachinin – School of Physics and Engineering, ITMO University, St. Petersburg, 197101, Russia

Yuri A. Mezenov – School of Physics and Engineering, ITMO University, St. Petersburg, 197101, Russia

Nikita K. Kulachenkov – School of Physics and Engineering, ITMO University, St. Petersburg, 197101, Russia

Maria Timofeeva – School of Physics and Engineering, ITMO University, St. Petersburg, 197101, Russia

Valentina Ivashchenko – School of Physics and Engineering, ITMO University, St. Petersburg, 197101, Russia

Anastasia A. Yakubova – Peter the Great St. Petersburg Polytechnic University, St. Petersburg 195251, Russia

Alexander S. Timin – School of Physics and Engineering, ITMO University, St. Petersburg, 197101, Russia

Sergei A. Shipilovskikh – School of Physics and Engineering, ITMO University, St. Petersburg, 197101, Russia

Dmitry I. Pavlov – Nikolaev Institute of Inorganic Chemistry SB RAS, Novosibirsk 630090, Russia

Andrei S. Potapov – Nikolaev Institute of Inorganic Chemistry SB RAS, Novosibirsk 630090, Russia

Jiang Gong – Key Laboratory of Material Chemistry for Energy Conversion and Storage, School of Chemistry and Chemical Engineering, Huazhong University of Science and Technology, Wuhan 430074, China

Laura Khamkhash – Department of Chemistry, Nazarbayev University, Astana 010000, Kazakhstan

Timur Sh. Atabaev – Department of Chemistry, Nazarbayev University, Astana 010000, Kazakhstan

Stéphanie Bruyere – Université de Lorraine, CNRS, IJL, F-54011 Nancy, France

Present Addresses

Nikita K. Kulachenkov, Present address: Department of Mechanical Engineering, Tufts University, Medford, USA.

Notes

The authors declare no competing financial interest.

ACKNOWLEDGMENT

V.A.M. acknowledges the financial support from the Russian Science foundation (Grant Numb. 22-72-10027 “Flexible hybrid materials as active layer in memory devices”) and Priority 2030 Federal Academic Leadership Program. E.V.G thanks the financial support from the Russian Foundation for Basic Research (Grant Numb. 21-52-15029). S.A.S. acknowledges the financial support by the Government of the Russian Federation through the ITMO Fellowship and Professorship Program. A.A.Y. acknowledges the Ministry of science and higher education of Russian Federation FSEG-2022-0012 (CLSM imaging, synthesis of fluorescent dyes).

REFERENCES

[1] Bennett, T. D.; Cheetham, A. K.; Fuchs, A. H.; Coudert, F.-X. Interplay Between Defects, Disorder and Flexibility in Metal-Organic Frameworks. *Nat. Chem*. **2016**, *9*, 11–16.

[2] Bennett, T. D.; Coudert, F.-X.; James, S. L.; Cooper, A. I. The Changing State of Porous Materials. *Nat. Mater*. **2021**, *20*, 1179–1187.

[3] Van Vleet, M. J.; Weng, T.; Li, X.; Schmidt, J. R. In Situ, Time-Resolved, and Mechanistic Studies of Metal–Organic Framework Nucleation and Growth. *Chem. Rev.* **2018**, *118*, 3681–3721.

[4] Zhang, X.; Chen, Z.; Liu, X.; Hanna, S. L.; Wang, X.; Taheri-Ledari, R.; Maleki, A.; Li, P.; Farha, O. K. A Historical Overview of the Activation and Porosity of Metal–Organic Frameworks. *Chem. Soc. Rev*. **2020**, *49*, 7406–7427.

[5] Zhou, H. C.; Long, J. R.; Yaghi, O. M. Introduction to Metal–Organic Frameworks. *Chem. Rev.* **2012**, *112*, 673–674.

[6] Li, H.; Wang, K.; Sun, Y.; Lollar, C. T.; Li, J.; Zhou, H.-C. Recent Advances in Gas Storage and Separation Using Metal–Organic Frameworks. *Mater. Today* **2018**, *21*, 108–121.

[7] Zhao, Y.; Song, Z.; Li, X.; Sun, Q.; Cheng, N.; Lawes, S.; Sun, X. Metal Organic Frameworks for Energy Storage and Conversion. *Energy Storage Mater.* **2016**, *2*, 35–62.

[8] Pascanu, V.; González Miera, G.; Inge, A. K.; Martín-Matute, B. Metal–Organic Frameworks as Catalysts for Organic Synthesis: A Critical Perspective. *J. Am. Chem. Soc*. **2019**, *141*, 7223–7234.

[9] Ma, X.; Lepoitevin, M.; Serre, C. Metal–Organic Frameworks Towards Bio-Medical Applications. *Mater. Chem. Front*. **2021**, *5*, 5573–5594.

[10] Mezenov, Y. A.; Krasilin, A. A.; Dzyuba, V. P.; Nominé, A.; Milichko, V. A. Metal–Organic Frameworks in Modern Physics: Highlights and Perspectives. *Adv. Sci.* **2019**, *6*, 1900506.

[11] Zhou, H.; Ren, Z.; Xu, C.; Xu, L.; Lee, C. MOF/Polymer-Integrated Multi-Hotspot Mid-Infrared Nanoantennas for Sensitive Detection of CO_2 Gas. *Nano-Micro Lett*. **2022**, *14*, 207.

[12] Kaneti, Y. V.; Tang, J.; Salunkhe, R. R.; Jiang, X.; Yu, A.; Wu, K. C.-W.; Yamauchi, Y. Nanoarchitectured Design of Porous Materials and Nanocomposites from Metal-Organic Frameworks. *Adv. Mater.* **2016**, *29*, 1604898.

[13] Guan, B. Y.; Yu, X. Y.; Wu, H. B.; Lou, X. W. D. Complex Nanostructures from Materials Based on Metal-Organic Frameworks for Electrochemical Energy Storage and Conversion. *Adv. Mater.* **2017**, *29*, 1703614.

[14] Indra, A.; Song, T.; Paik, U. Metal Organic Framework Derived Materials: Progress and Prospects for the Energy Conversion and Storage. *Adv. Mater.* **2018**, *30*, 1705146.

[15] Qiu, C.; Qian, K.; Yu, J.; Sun, M.; Cao, S.; Gao, J.; Yu, R.; Fang, L.; Yao, Y.; Lu, X.; Li, T.; Huang, B.; Yang, S. MOF-Transformed In_2O_3-x@C Nanocorn Electrocatalyst for Efficient CO2 Reduction to HCOOH. *Nano-Micro Lett*. **2022**, *14*, 167.

[16] Huang, X.; Li, L.; Zhao, S.; Tong, L.; Li, Z.; Peng, Z.; Lin, R.; Zhou, L.; Peng, C.; Xue, K. H.; Chen, L.; Cheng, G. J.; Xiong, Z.; Ye, L. MOF-Like 3D Graphene-Based Catalytic

Membrane Fabricated by One-Step Laser Scribing for Robust Water Purification and Green Energy Production. *Nano-Micro Lett*. **2022**, *14*, 174.

[17] Luo, Y.; Ahmad, M.; Schug, A.; Tsotsalas, M. Rising Up: Hierarchical Metal–Organic Frameworks in Experiments and Simulations. *Adv. Mater*. **2019**, *31*, 1901744.

[18] Thiruvengadathan, R.; Korampally, V.; Ghosh, A.; Chanda, N.; Gangopadhyay, K.; Gangopadhyay, S. Nanomaterial Processing Using Self-Assembly-Bottom-up Chemical and Biological Approaches. *Rep. Prog. Phys*. **2013**, *76*, 066501.

[19] Chai, L.; Zhang, L.; Wang, X.; Xu, L.; Han, C.; Li, T.-T.; Hu, Y.; Qian, J.; Huang, S. Bottom-up Synthesis of MOF-Derived Hollow N-Doped Carbon Materials for Enhanced ORR Performance. *Carbon* **2019**, *146*, 248–256.

[20] Gadipelli, S.; Li, Z.; Lu, Y.; Li, J.; Guo, J.; Skipper, N. T.; Shearing, P. R.; Brett, D. J. L. Size- Related Electrochemical Performance in Active Carbon Nanostructures: A MOFs- Derived Carbons Case Study. *Adv. Sci*. **2019**, *6*, 1901517.

[21] Jagadeesh, R. V.; Murugesan, K.; Alshammari, A. S.; Neumann, H.; Pohl, M.-M.; Radnik, J.; Beller, M. MOF-Derived Cobalt Nanoparticles Catalyze a General Synthesis of Amines. *Science* **2017**, *358*, 326–332.

[22] Yang, S.; Peng, L.; Bulut, S.; Queen, W. L. Recent Advances of MOFs and MOF-Derived Materials in Thermally Driven Organic Transformations. *Chem. - Eur. J.* **2018**, *25*, 2161–2178.

[23] Xing, L.; Li, M.; Li, M.; Xu, T.; Li, Y.; Qi, T.; Li, H.; Hu, Z.; Hao, G. P.; Zhang, S.; James, T. D.; Mao, B.; Wang, L. MOF-Derived Robust and Synergetic Acid Sites Inducing C–N

Bond Disruption for Energy-Efficient CO_2 Desorption. *Environ. Sci. Technol.* **2022**, *56*, 17936–17945.

[24] Dou, X.; Liu, J.; Gong, X.; Jiang, H.; Deng, H. Laser Driven Conversion of MOFs to Rare Earth Metal Oxide Nanoparticles. *APL Mater*. **2022**, *10*, 041110.

[25] Jiang, H.; Jin, S.; Wang, C.; Ma, R.; Song, Y.; Gao, M.; Liu, X.; Shen, A.; Cheng, G. J.; Deng, H. Nanoscale Laser Metallurgy and Patterning in Air Using MOFs. *J. Am. Chem. Soc*. **2019**, *141*, 5481–5489.

[26] Guo, S.; Zhao, Y.; Yuan, H.; Wang, C.; Jiang, H.; Cheng, G. J. Ultrafast Laser Manufacture of Stable, Efficient Ultrafine Noble Metal Catalysts Mediated with MOF Derived High Density Defective Metal Oxides. *Small* **2020**, *16*, 2000749.

[27] Tang, Y.; Zheng, H.; Wang, Y.; Zhang, W.; Zhou, K. Laser- Induced Annealing of Metal–Organic Frameworks on Conductive Substrates for Electrochemical Water Splitting. *Adv. Funct. Mater*. **2021**, *31*, 2102648.

[28] Ribeiro, E. L.; Davis, E. M.; Mokhtarnejad, M.; Hu, S.; Mukherjee, D.; Khomami, B. MOF-Derived PtCo/Co3O4 Nanocomposites in Carbonaceous Matrices as High-Performance ORR Electrocatalysts Synthesized via Laser Ablation Techniques. *Catal. Sci. Technol*. **2021**, *11*, 3002–3013.

[29] Mingabudinova, L. R.; Zalogina, A. S.; Krasilin, A. A.; Petrova, M. I.; Trofimov, P.; Mezenov, Y. A.; Ubyivovk, E. V.; Lönnecke, P.; Nominé, A.; Ghanbaja, J.; Belmonte, T.; Milichko, V. A. Laser Printing of Optically Resonant Hollow Crystalline Carbon Nanostructures from 1D and 2D Metal–Organic Frameworks. *Nanoscale* **2019**, *11*, 10155–10159.

[30] Jiang, H.; Tong, L.; Liu, H.; Xu, J.; Jin, S.; Wang, C.; Hu, X.; Ye, L.; Deng, H.; Cheng, G. J. Graphene-Metal-Metastructure Monolith via Laser Shock-Induced Thermochemical Stitching of MOF Crystals. *Matter* **2020**, *2*, 1535–1549.

[31] Ma, R.; Jiang, H.; Wang, C.; Zhao, C.; Deng, H. Multivariate MOFs for Laser Writing of Alloy Nanoparticle Patterns. *Chem. Commun.* **2020**, *56*, 2715–2718.

[32] Kulachenkov, N. K.; Bruyere, S.; Sapchenko, S. A.; Mezenov, Y. A.; Sun, D.; Krasilin, A. A.; Nominé, A.; Ghanbaja, J.; Belmonte, T.; Fedin, V. P.; Pidko, E. A.; Milichko, V. A. Ultrafast Melting of Metal–Organic Frameworks for Advanced Nanophotonics. *Adv. Funct. Mater*. **2019**, *30*, 1908292.

[33] Pavlov, D. I.; Ryadun, A. A.; Potapov, A. S.; A Zn(II)-Based Sql Type 2D Coordination Polymer as a Highly Sensitive and Selective Turn-On Fluorescent Probe for Al^{3+}. *Molecules* **2021**, *26*, 7392.

[34] Joglekar, A. P.; Liu, H. H.; Meyhöfer, E.; Mourou, G.; Hunt, A. J. Optics at Critical Intensity: Applications to Nanomorphing. *Proc. Natl. Acad. Sci. U.S.A*. **2004**, *101*, 5856-5861.

[35] Stoian, R.; Ashkenasi, D.; Rosenfeld, A.; Campbell, E. E. B. Coulomb Explosion in Ultrashort Pulsed Laser Ablation of Al_2O_3. *Phys. Rev. B* **2000**, *62*, 13167.

[36] Otto, M. R.; Pöhls, J. H.; René de Cotret, L. P.; Stern, M. J.; Sutton, M.; Siwick, B. J.; Mechanisms of Electron-Phonon Coupling Unraveled in Momentum and Time: The Case of Soft Phonons in $TiSe_2$. *Sci. Adv*. **2021**, *7*, eabf2810.

[37] Shirk, M. D.; Molian, P. A. A Review of Ultrashort Pulsed Laser Ablation of Materials. *J. Laser Appl.* **1998**, *10*, 18–28.

[38] Semaltianos, N. G. Nanoparticles by Laser Ablation. *Crit. Rev. Solid State Mater. Sci.* **2010**, *35*, 105–124.

[39] Ravi-Kumar, S.; Lies, B.; Lyu, H.; Qin, H. Laser Ablation of Polymers: A Review. *Procedia Manufacturing* **2019**, *34*, 316–327.

[40] Wu, Y.; Huang, Z.; Jiang, H.; Wang, C.; Zhou, Y.; Shen, W.; Xu, H.; Deng, H. Facile Synthesis of Uniform Metal Carbide Nanoparticles from Metal–Organic Frameworks by Laser Metallurgy. *ACS Appl. Mater. Interfaces* **2019**, *11*, 44573–44581.

[41] Lam, D. V.; Dung, D. T.; Kim, J.-H.; Kim, H.; Lee, S.-M. Laser-Induced Sulfurization of Nickel-Based Metal-Organic Frameworks for Highly Stable Phase-Engineered Energy Materials. *Chem. Eng. J.* **2022**, *437*, 135237.

[42] Pečinka, L.; Peña-Méndez, E. M.; Conde-González, J. E.; Havel, J. Laser Ablation Synthesis of Metal-Doped Gold Clusters from Composites of Gold Nanoparticles with Metal Organic Frameworks. *Sci. Rep*. **2021**, *11*, 4656.

[43] Zhang, W.; Yan, W.; Jiang, H.; Wang, C.; Zhou, Y.; Ke, F.; Cong, H.; Deng, H. Uniform Bi–Sb Alloy Nanoparticles Synthesized from MOFs by Laser Metallurgy for Sodium-Ion Batteries. *ACS Sustainable Chem. Eng.* **2019**, *8*, 335–342.

[44] Wei, Y.; Haoqing J.; Wendi, Y.; Chengbin, Z.; Yucong, X.; Hengjiang, C.; Lin, T.; Gary, J. Ch.; Jianhua, H.; Hexiang, D.; High-Entropy-Alloy Nanoparticles Synthesized by Laser Metallurgy Using a Multivariate MOF. *Mater. Chem. Front.* **2022**, *6*, 2796–2802.

[45] Van Lam, D.; Sohail, M.; Kim, J.-H.; Lee, H. J.; Han, S. O.; Shin, J.; Kim, D.; Kim, H.; Lee, S.-M. Laser Synthesis of MOF-Derived Ni@Carbon for High-Performance Pseudocapacitors. *ACS Appl. Mater. Interfaces* **2020**, *12*, 39154–39162.

[46] Wang, K.; Feng, L.; Yan, T.; Wu, S.; Joseph, E. A.; Zhou, H. Rapid Generation of Hierarchically Porous Metal–Organic Frameworks Through Laser Photolysis. *Angew. Chem., Int. Ed*. **2020**, *59*, 11349–11354.

[47] Zhestkij, N.; Efimova, A.; Rzhevskiy, S.; Kenzhebayeva, Y.; Bachinin, S.; Gunina, E.; Sergeev, M.; Dyachuk, V.; Milichko, V. A. Reversible and Irreversible Laser Interference Patterning of MOF Thin Films. *Crystals* **2022**, *12*, 846.

[48] Mezenov, Y. A.; Bruyere, S.; Krasilin, A.; Khrapova, E.; Bachinin, S. V.; Alekseevskiy, P. V.; Shipilovskikh, S.; Boulet, P.; Hupont, S.; Nomine, A.; Vigolo, B.; Novikov, A. S.; Belmonte, T.; Milichko, V. A. Insights into Solid-To-Solid Transformation of MOF Amorphous Phases. *Inorg. Chem*. **2022**, *61*, 13992–14003.

[49] Howarth, A. J.; Liu, Y.; Li, P.; Li, Z.; Wang, T. C.; Hupp, J. T.; Farha, O. K. Chemical, Thermal and Mechanical Stabilities of Metal–Organic Frameworks. *Nat. Rev. Mater*. **2016**, *1*, 15018.

[50] Wu, Y.-P.; Zhou, W.; Dong, W.-W.; Zhao, J.; Qiao, X.-Q.; Hou, D.-F.; Li, D.-S.; Zhang, Q.; Feng, P. Temperature-Controlled Synthesis of Porous CuO Particles with Different

Morphologies for Highly Sensitive Detection of Triethylamine. *Cryst. Growth Des*. **2017**, *17*, 2158–2165.

[51] Basnayake, S. A.; Su, J.; Zou, X.; Balkus, K. J. Carbonate-Based Zeolitic Imidazolate Framework for Highly Selective CO_2 Capture. *Inorg. Chem*. **2015**, *54*, 1816–1821.

[52] Cavka, J. H.; Jakobsen, S.; Olsbye, U.; Guillou, N.; Lamberti, C.; Bordiga, S.; Lillerud, K. P. A New Zirconium Inorganic Building Brick Forming Metal Organic Frameworks with Exceptional Stability. *J. Am. Chem. Soc*. **2008**, *130*, 13850–13851.

[53] Mezenov, Y. A.; Bruyere, S.; Kulachenkov, N. K.; Yankin, A. N.; Rzhevskiy, S. S.; Alekseevskiy, P. V.; Gilemkhanova, V. D.; Bachinin, S. V.; Dyachuk, V.; Krasilin, A. A.; Zollinger, J.; Belmonte, T.; Nominé, A.; Milichko, V. A. Probing the Dynamics of Cu Nanoparticle Growth Inside Metal-Organic Frameworks Upon Electron Beam Irradiation. *Photon. Nanostruct. Fund. App*. **2020**, *41*, 100832.

[54] Thapliyal, V.; Alabdulkarim, M. E.; Whelan, D. R.; Mainali, B.; Maxwell, J. L. A Concise Review of the Raman Spectra of Carbon Allotropes. *Diamond Related Mater*. **2022**, *127*, 109180.

[55] Mezenov, Y. A.; Kulachenkov, N. K.; Yankin, A. N.; Rzhevskiy, S. S.; Alekseevskiy, P. V.; Gilemkhanova, V. D.; Bachinin, S. V.; Dyachuk, V.; Milichko, V. A. Polymer Matrix Incorporated with ZIF-8 for Application in Nonlinear Optics. *Nanomaterials* **2020**, *10*, 1036.

[56] Han, S.; Zhang, H.; Zhang, J.; Xie, Y.; Liu, L.; Wang, H.; Li, X.; Liu, W.; Tang, Y. Fabrication, Gradient Extraction and Surface Polarity-Dependent Photoluminescence of Cow Milk-Derived Carbon Dots. *RSC Adv.* **2014**, *4*, 58084–58089.

[57] Kulachenkov, N.; Haar, Q.; Shipilovskikh, S.; Yankin, A.; Pierson, J.; Nominé, A.; Milichko, V. A. MOF- Based Sustainable Memory Devices. *Adv. Funct. Mater*. **2021**, *32*, 2107949.

[58] Shanks, K.; Senthilarasu, S.; Mallick, T. K. Optics for concentrating photovoltaics: Trends, limits and opportunities for materials and design. *Renew. Sust. Energy Rev*. **2016**, *60*, 394-407.

[59] Milichko, V. A.; Makarov, S. V.; Yulin, A. V.; Vinogradov, A. V.; Krasilin, A. A.; Ushakova, E.; Dzyuba, V. P.; Hey-Hawkins, E.; Pidko, E. A.; Belov, P. A. van der Waals Metal-Organic Framework as an Excitonic Material for Advanced Photonics. *Adv. Mater*. **2017**, *29*, 1606034.

[60] Kulachenkov, N. K.; Sun, D.; Mezenov, Y. A.; Yankin, A. N.; Rzhevskiy, S.; Dyachuk, V.; Nominé, A.; Medjahdi, G.; Pidko, E. A.; Milichko, V. A. Photochromic Free MOF-Based Near-Infrared Optical Switch. *Angew. Chemie Int. Ed.* **2020**, *59*, 15522-15526.

[61] Kulachenkov, N.; Barsukova, M.; Alekseevskiy, P.; Sapianik, A. A.; Sergeev, M.; Yankin, A.; Krasilin, A. A.; Bachinin, S.; Shipilovskikh, S.; Poturaev, P.; Medvedeva, N.; Denislamova, E.; Zelenovskiy, P. S.; Shilovskikh, V. V.; Kenzhebayeva, Y.; Efimova, A.; Novikov, A. S.; Lunev, A.; Fedin, V. P.; Milichko, V. A. Dimensionality Mediated Highly Repeatable and Fast Transformation of Coordination Polymer Single Crystals for All-Optical Data Processing. *Nano Lett*. **2022,** *22*, 6972-6981.

[62] Peiris, S.; McMurtrie, J.; Zhu, H. Y. Metal Nanoparticle Photocatalysts: Emerging Processes for Green Organic Synthesis. *Catal. Sci. Technol*. **2016**, *6*, 320-338.

[63] Xu, S.; Chansai, S.; Stere, C.; Inceesungvorn, B.; Goguet, A.; Wangkawong, K.; Taylor, S. F. R.; Al-Janabi, N.; Hardacre, C.; Martin, P. A.; Fan, X. Sustaining Metal–Organic Frameworks for Water–Gas Shift Catalysis by Non-Thermal Plasma. *Nat. Catal.* **2019**, *2*, 142–148.

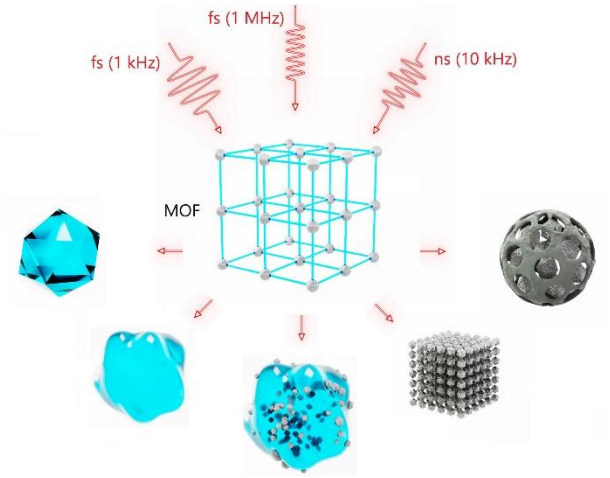

Figure 1. Scheme of fs to ns laser conversion of MOF to produce different derivatives.

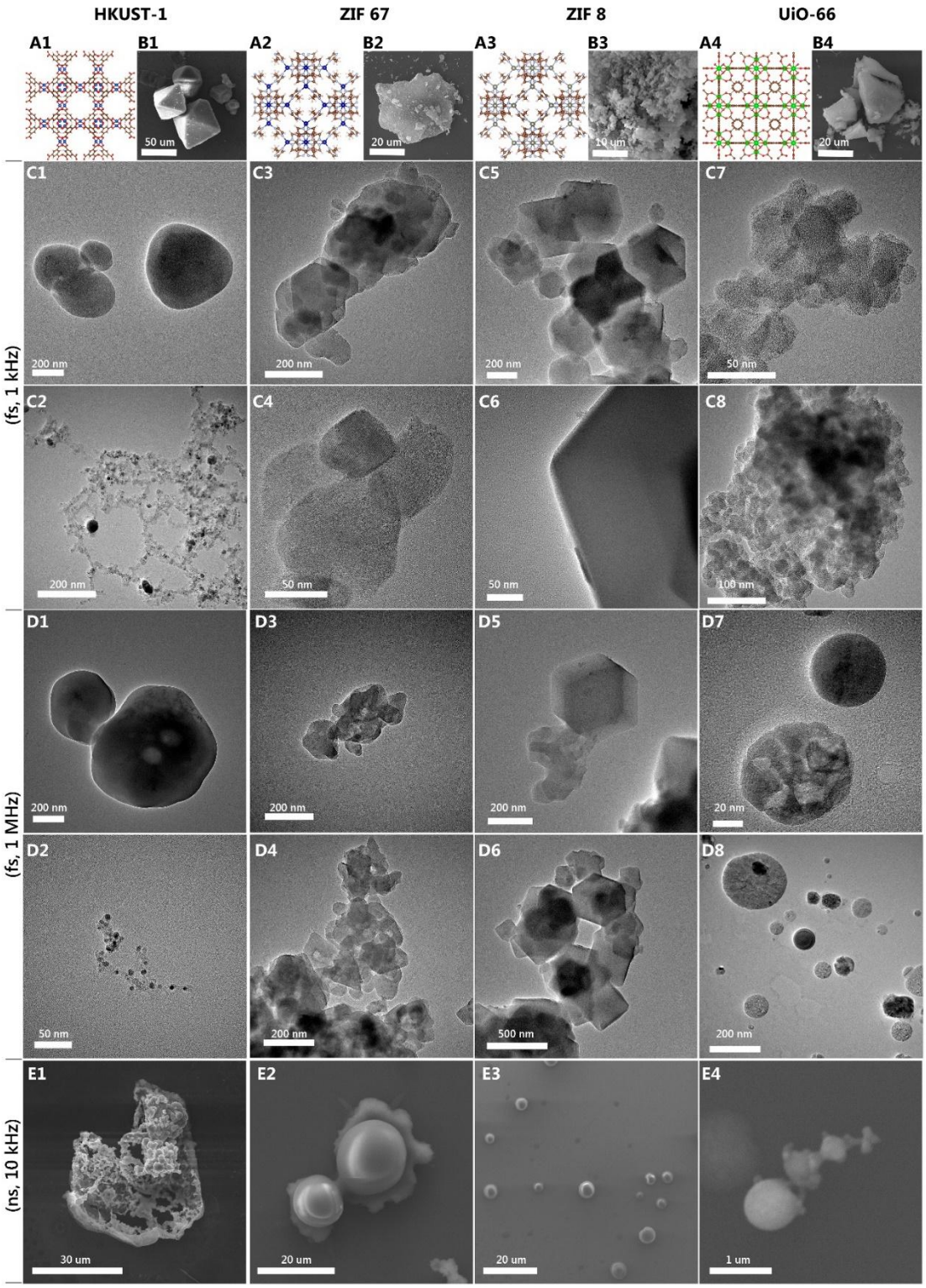

Figure 2. Electron microscopy of MOF derivatives. (A) A series of MOFs structure: HKUST-1 (A1), ZIF 67 (A2), ZIF 8 (A3), and UiO-66 (A4) arranged in order of increasing the thermal

resistance. (B) Corresponding SEM micrographs of the initial MOF crystals. (C) TEM micrographs of the results of femtosecond (1 kH) laser conversion of MOFs: (C1,C2) HKUST-1 DER (fs, 1 kHz), (C3,C4) ZIF-67 DER (fs, 1 kHz), (C5,C6) ZIF-8 DER (fs, 1 kHz), (C7,C8) UiO-66 DER (fs, 1 kHz). (D) TEM micrographs of the results of femtosecond (1 MH) laser conversion of MOFs: (D1,D2) HKUST-1 DER (fs, 1 MHz), (D3,D4) ZIF-67 DER (fs, 1 MHz), (D5,D6) ZIF-8 DER (fs, 1 MHz), (D7,D8) UiO-66 DER (fs, 1 MHz). (E) SEM micrographs of the results of nanosecond (10 kH) laser conversion of MOFs: (E1) HKUST-1 DER (ns, 10 kHz), (E2) ZIF-67 DER (ns, 10 kHz), (E3) ZIF-8 DER (ns, 10 kHz), (E4) UiO-66 DER (ns, 10 kHz).

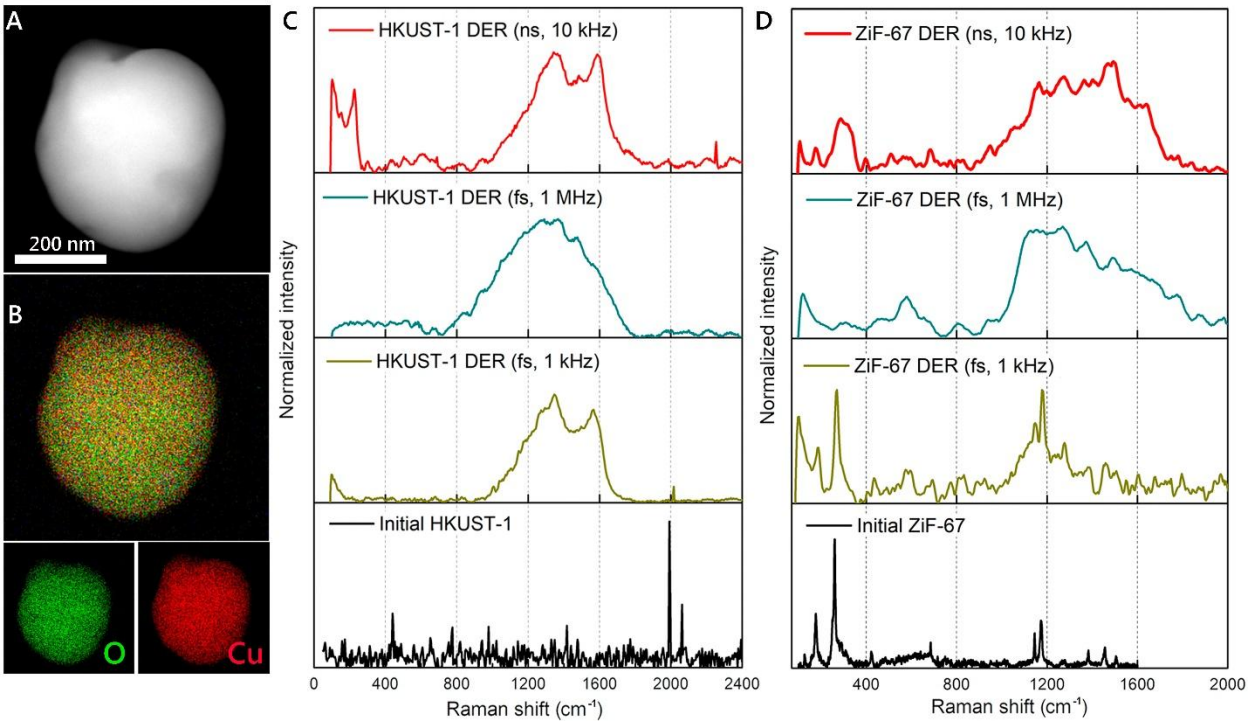

Figure 3. Structural characterization of MOFs. (A) STEM micrograph and (B) STEM EDX map of HKUST-1 DER (fs, 1 kHz). (C,D) Raman spectra for HKUST-1 and ZIF-67 derivatives obtained by fs and ns laser conversion regimes.

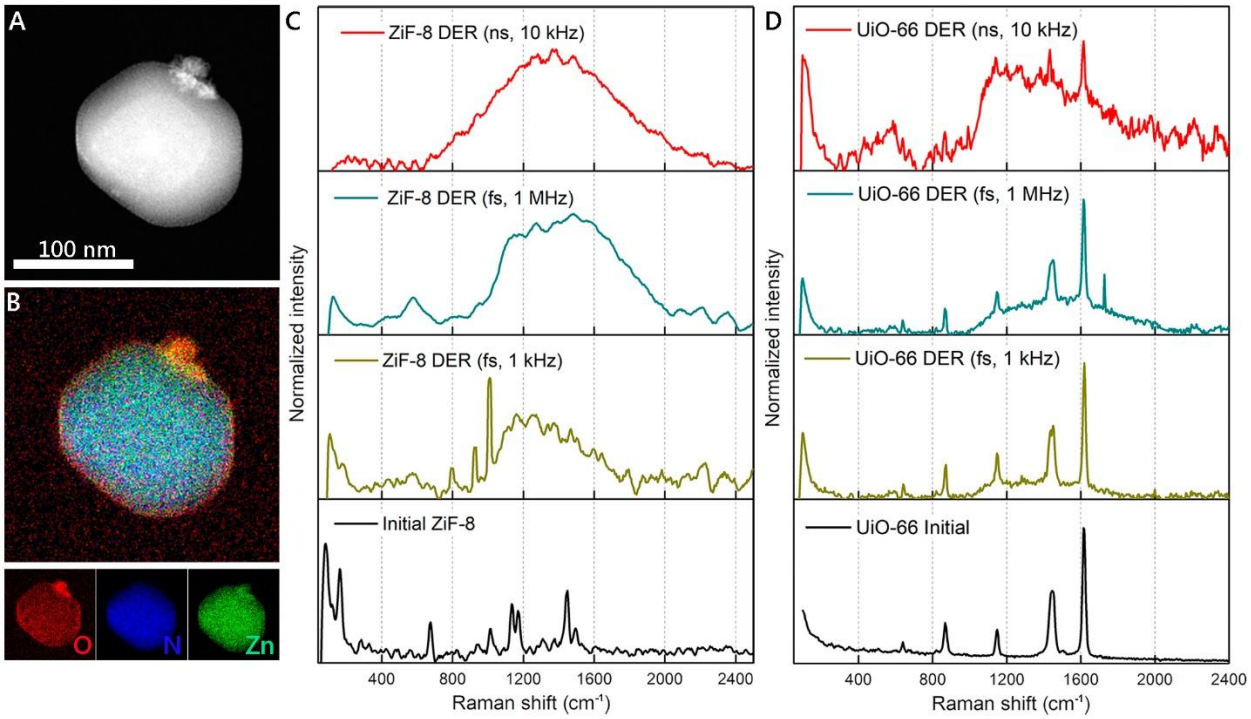

Figure 4. Structural characterization of MOFs. (A) STEM micrograph and (B) STEM EDX map of ZIF-8 DER (fs, 1 MHz). (C,D) Raman spectra for ZIF-8 and UiO-66 derivatives obtained by fs and ns laser conversion regimes.

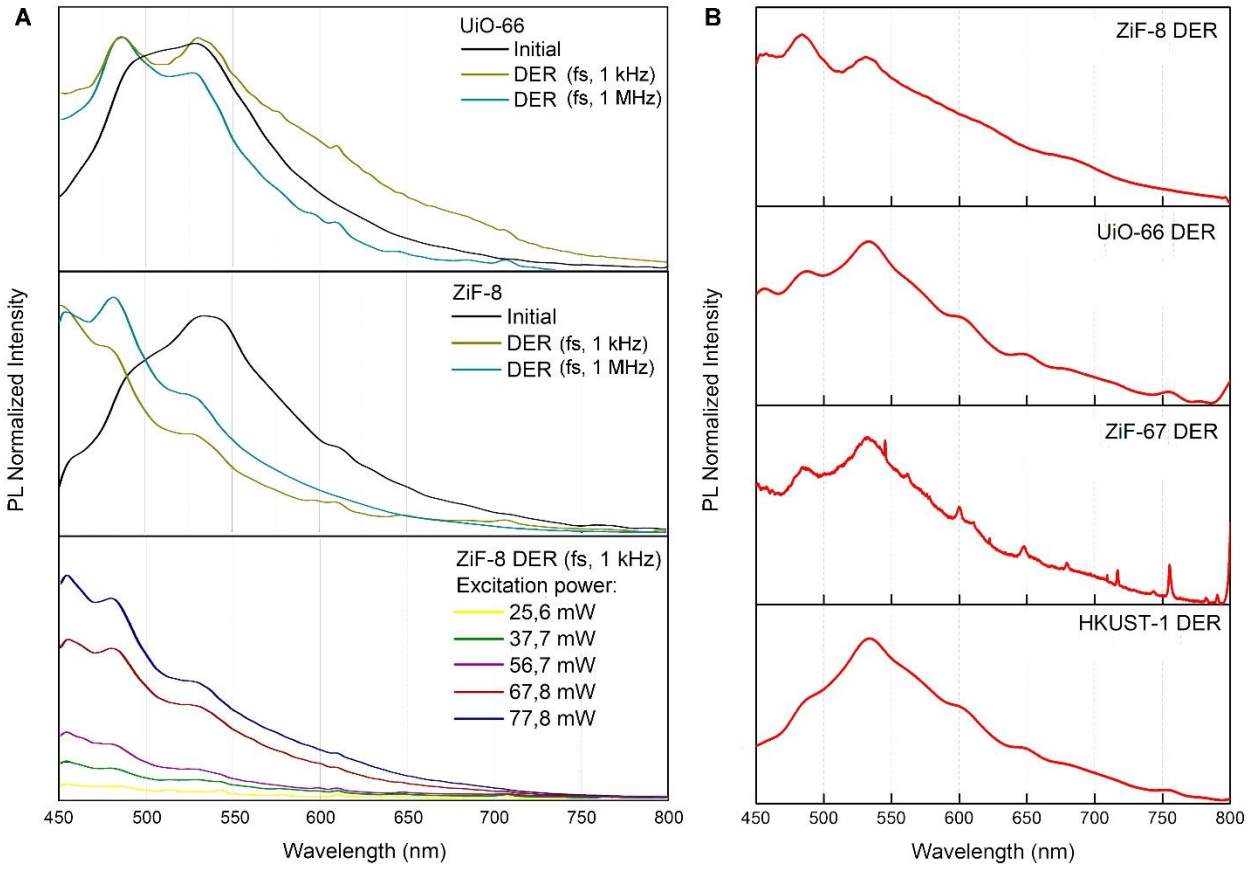

Figure 5. Photoluminescence of MOF derivatives. (A) PL from the initial MOF crystals (UiO-66 and ZIF-8) and their derivatives, obtained by fs laser conversion, excited by 400 nm. Power dependence of PL from ZIF-8 DER (fs, 1 kH). (B) PL from the derivatives of MOFs, obtained by ns laser conversion (10 kHz), excited by 400 nm.

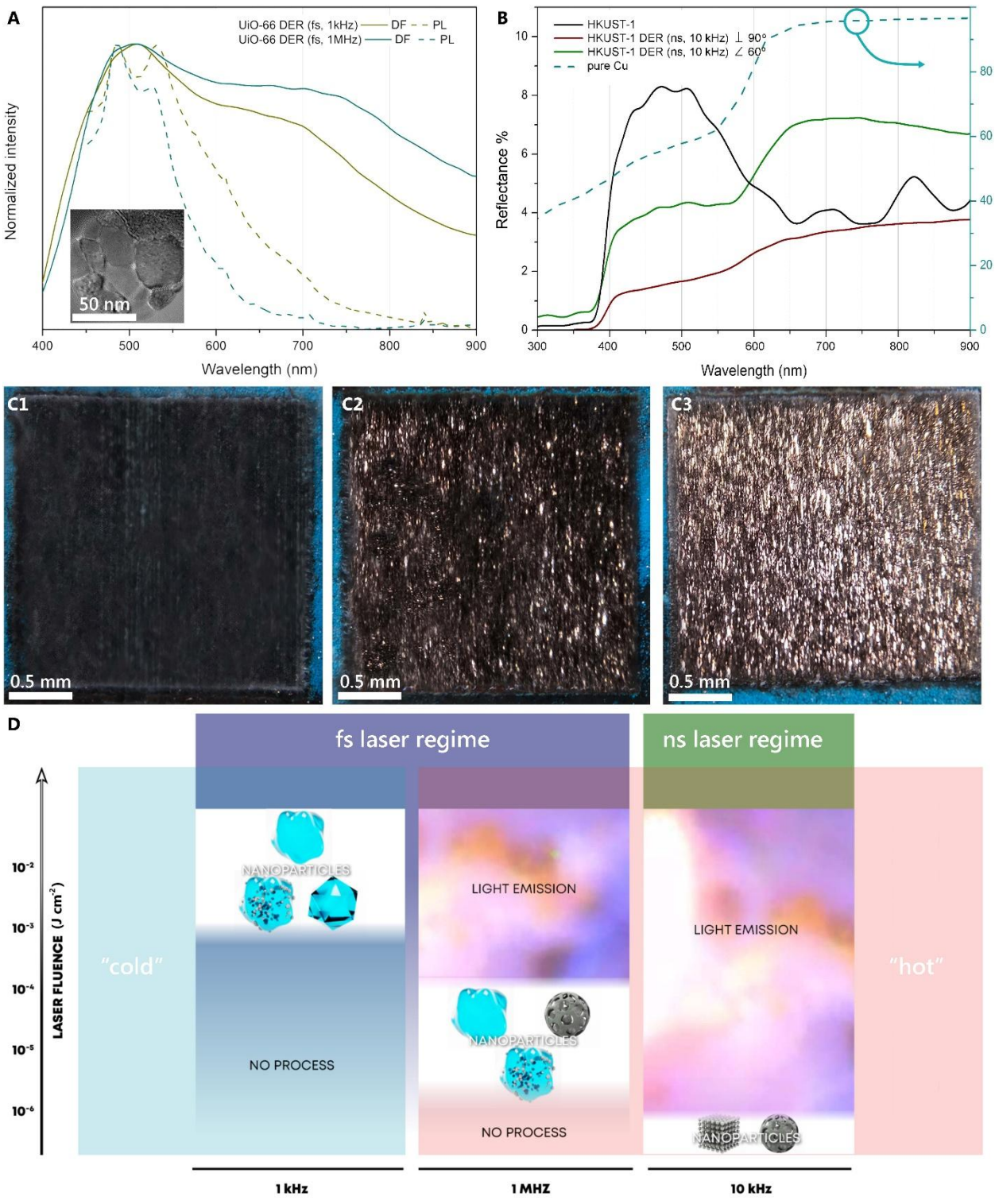

Figure 6. (A) PL and scattering (in dark field geometry, DF) spectra from UiO-66 DER (fs, 1 kHz) and (fs, 1 MHz). Inset: TEM micrograph of the corresponding nanometer scale UiO-66

DER (fs, 1 MHz). (B) Reflectance from the surface of HKUST-1 initial crystal (black curve), pure Cu substrate (dashed curve) and 4 cm^2 MOF derivatives with corresponding optical images, obtained at different angles (perpendicular to the surface and to 60° relative to the surface normal): (C1) optical image of the fs laser conversion (fs, 1 kHz), (C2) optical image of the fs laser conversion (fs, 1 MHz), and (C3) optical image of the ns laser conversion (ns, 10 kHz) of HKUST-1. (D) Space of "laser parameters vs. MOF structure" for the prediction of the structure of the MOF derivatives from nano to centimeter scales.

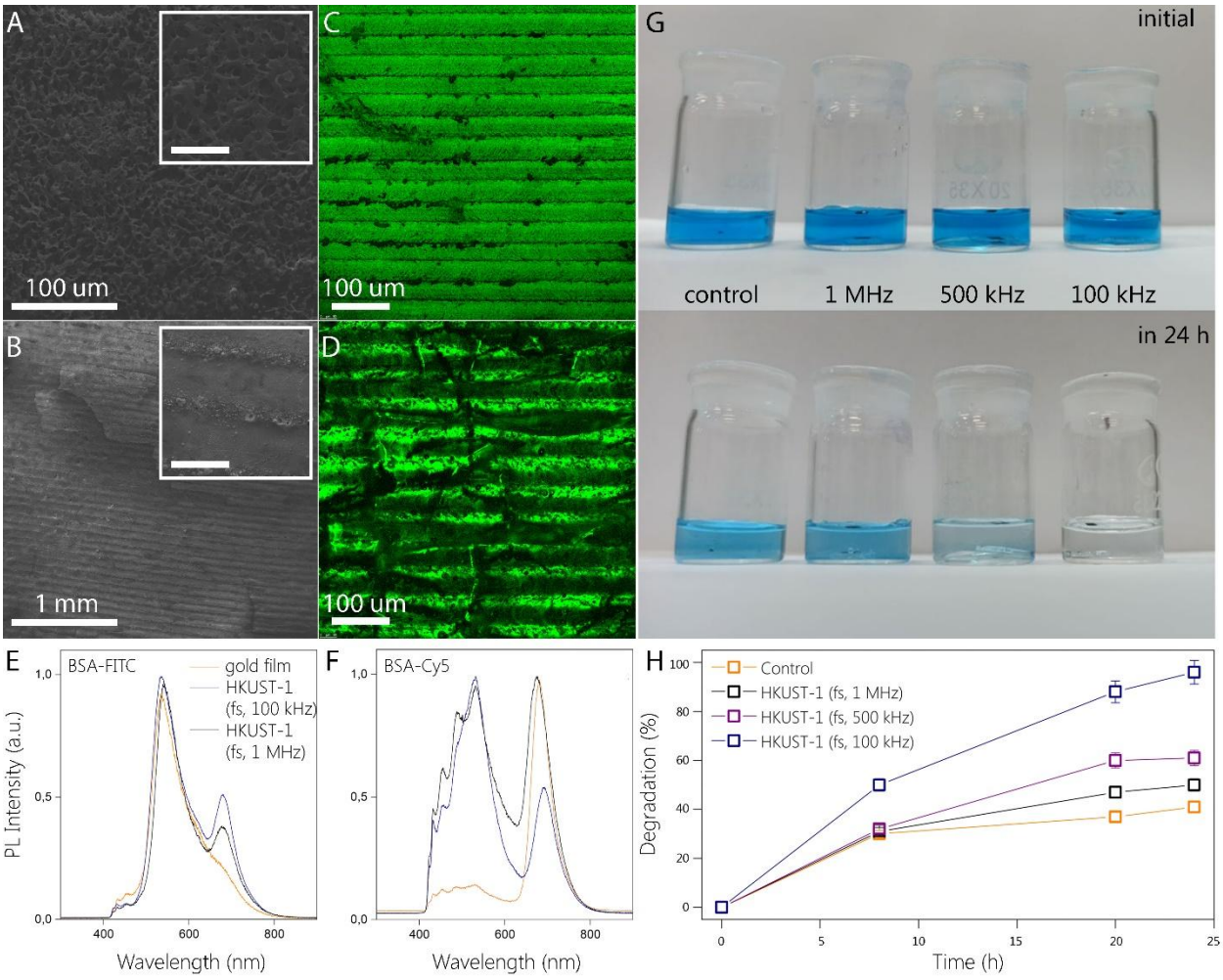

Figure 7. (A,B) SEM and (C,D) CLSM images of 4 cm^2 surfaces based on HKUST-1 after fs laser conversion with 100 kHz (A,C) and 1 MHz (B,D) repetition rates. Inset: Scale bars, 100

μm. (E,F) PL spectra for BSA-FITC (E) and BSA-Cy5 (F) conjugates covering HKUST-1 DER (fs, 100 kHz), HKUST-1 DER (fs, 1 MHz) surfaces, and a gold film as a reference. (G,H) Degradation of Rh800 in an aqueous solution with the presence of HKUST-1 DER (fs, 100 kHz), (fs, 500 kHz), and (fs, 1 MHz) surfaces.

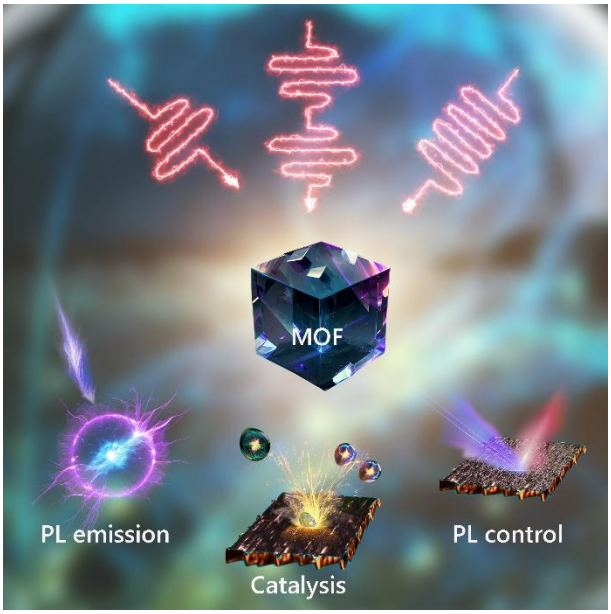

Table Of Contents